Microbiome

RESEARCH

Open Access

# Dietary emulsifier carboxymethylcellulose-induced gut dysbiosis and SCFA reduction aggravate acute pancreatitis through classical monocyte activation

Yongpu Feng[1,2†], Wenjin Chen[3†], Jiayu Chen[4†], Fengyuan Sun[1,2†], Fanyang Kong[1,2†], Lei Li[5†], Yating Zhao[1], Shouxin Wu[6], Zhaoshen Li[4*], Yiqi Du[2*] and Xiangyu Kong[1*]

## Abstract

**Objective** Carboxymethylcellulose (CMC), one of the most common emulsifiers used in the food industry, has been reported to promote chronic inflammatory diseases, but its impact on acute inflammatory diseases, e.g., acute pancreatitis (AP), remains unclear. This study investigates the detrimental effects of CMC on AP and the potential for mitigation through *Akkermansia muciniphila* or butyrate supplementation.

**Design** C57BL/6 mice were given pure water or CMC solution (1%) for 4 weeks and then subjected to caerulein-induced AP. The pancreas, colon, and blood were sampled for molecular and immune parameters associated with AP severity. Gut microbiota composition was assessed using 16S rRNA gene amplicon sequencing. Fecal microbiota transplantation (FMT) was used to illustrate gut microbiota's role in mediating the effects of CMC on host mice. Additional investigations included single-cell RNA sequencing, monocytes-specific C/EBPδ knockdown, LPS blocking, fecal short-chain fatty acids (SCFAs) quantification, and *Akkermansia muciniphila* or butyrate supplementation. Finally, the gut microbiota of AP patients with different severity was analyzed.

**Results** CMC exacerbated AP with gut dysbiosis. FMT from CMC-fed mice transferred such adverse effects to recipient mice, while single-cell analysis showed an increase in classical monocytes in blood. LPS-stimulated C/EBPδ, caused by an impaired gut barrier, drives monocytes towards classical phenotype. LPS antagonist (eritoran), *Akkermansia muciniphila* or butyrate supplementation ameliorates CMC-induced AP exacerbation. Fecal *Akkermansia muciniphila* abundance was negatively correlated with AP severity in patients.

†Yongpu Feng, Wenjin Chen, Jiayu Chen, Fengyuan Sun, Fanyang Kong and Lei Li contributed equally to this work.

*Correspondence:
Zhaoshen Li
zhsl@vip.163.com
Yiqi Du
duyiqi@hotmail.com
Xiangyu Kong
xiangyukong185@hotmail.com
Full list of author information is available at the end of the article

**Conclusions** This study reveals the detrimental impact of CMC on AP due to gut dysbiosis, with *Akkermansia muciniphila* or butyrate offering potential therapeutic avenues for counteracting CMC-induced AP exacerbation.

## Introduction

Ultra-processed foods (UPFs), consumption of which characterize up to 60% of the Western diet, has increased dramatically since the mid-twentieth century and is associated with elevated incidence of various chronic inflammatory diseases, e.g., metabolic syndrome, cardiovascular disease, and cancer [1–3]. One prevalent characteristic of UPFs is the inclusion of one or more emulsifiers, which are utilized to disperse non-mixable components, ensuring the stability of functional ingredients and flavors in food and beverages while extending their shelf life. Carboxymethylcellulose (CMC) is one of the most common emulsifiers used in the food industry. Despite the lack of extensive safety testing, CMC was approved in the 1960s for use in foods at concentrations up to 2% (wt/wt) by regulatory agencies, including the US Food and Drug Administration and the European Commission [4]. One reason for assuming the safety of CMC, as well as certain other emulsifiers, is that they are poorly absorbed and primarily excreted in feces. However, recent researches demonstrated that CMC could influence both human microbiota composition and gene expression in vitro, and in mice, which has been found to contribute to the development of colitis or metabolic syndrome [4–7]. Most publications describe the effects of CMC as "mild" or "subtle," resulting in only "low-grade" and "chronic" inflammation. Nevertheless, as of now, no research has investigated the potential involvement of emulsifiers, such as CMC, in the development of acute systemic inflammation.

Acute pancreatitis (AP) is the most common cause of hospitalization with a gastrointestinal condition, which loads heavy burdens on the current healthcare system, and the incidence of AP is increasing annually both in the USA and worldwide [8]. Despite the generally mild clinical course observed in the majority of cases, a noteworthy one-fifth of AP patients develop severe systemic inflammation, leading to persistent organ failures and an associated mortality rate of approximately 20% [8]. The rising prevalence of AP, occurring against the backdrop of relatively stable human genetics, hints at the involvement of non-genetic factors—specifically, environmental factors—in the pathogenesis of AP. Notably, the surge in AP cases has been roughly paralleled by increased consumption of UPFs, raising the possibility that certain components, such as emulsifiers, in these foods may contribute to the promotion of AP.

CMC, among the most prevalent emulsifiers, has been extensively studied for its role in mediating the negative impacts of UPFs on human health [6, 9]. While direct evidence is absent, various lines of evidence strongly indicate the potential role of CMC in the pathogenesis of AP. Firstly, numerous studies propose a fundamental role for gut microbiota in AP development [10, 11], whereas CMC predominantly exerts detrimental impacts through inducing gut dysbiosis [5, 7]. Secondly, CMC exposure induces alterations in the fecal metabolome, such as short-chain fatty acids (SCFAs) and bile acids [5], both of which were involved in AP pathgenesis [10, 12]. Gaining insights into the promotive effects of CMC on AP will not only provide novel preventive strategies in AP treatment but will also fill the knowledge gap regarding whether CMC can promote acute systemic inflammation, offering additional evidence for potential adjustments in our policy on CMC.

As deleterious effects are expected, clinical trials of CMC intervention are not ethical, we employed a caerulein-induced AP mouse model to evaluate the negative impacts of CMC on AP. Fecal microbiota transplantation (FMT) to recipient mice successfully transferred the detrimental effects of CMC, indicating that such effects were mediated by gut dysbiosis. Notably, an abundance of *Akkermansia muciniphila* showed the most significant correlation with various parameters of AP severity. Reduced fecal *Akkermansia muciniphila* was mechanistically linked to SCFA reduction, gut barrier dysfunction, increased LPS leakage into the bloodstream, classical monocytes frequency elevation in blood, and ultimately, the worsening of AP.

## Results

### CMC exposure exacerbated caerulein-induced AP

To study the effect of CMC on AP, C57BL/6 mice were subjected to either pure water (PW) or CMC solution (1%) for 4 weeks, followed by intraperitoneal injection with caerulein (CAE) or normal saline (NS) (Fig. 1a). Mice in CMC + CAE group exhibited increased pancreas/body weight ratio, higher histologic score, raised serum amylase and lipase, as compared to mice in PW + CAE group (Fig. 1b–f). Additionally, mice in CMC + CAE group displayed higher serum proinflammatory cytokines IL-6 and TNF-α (Fig. 1g, h). These data collectively demonstrated that AP was significantly exacerbated after CMC exposure.

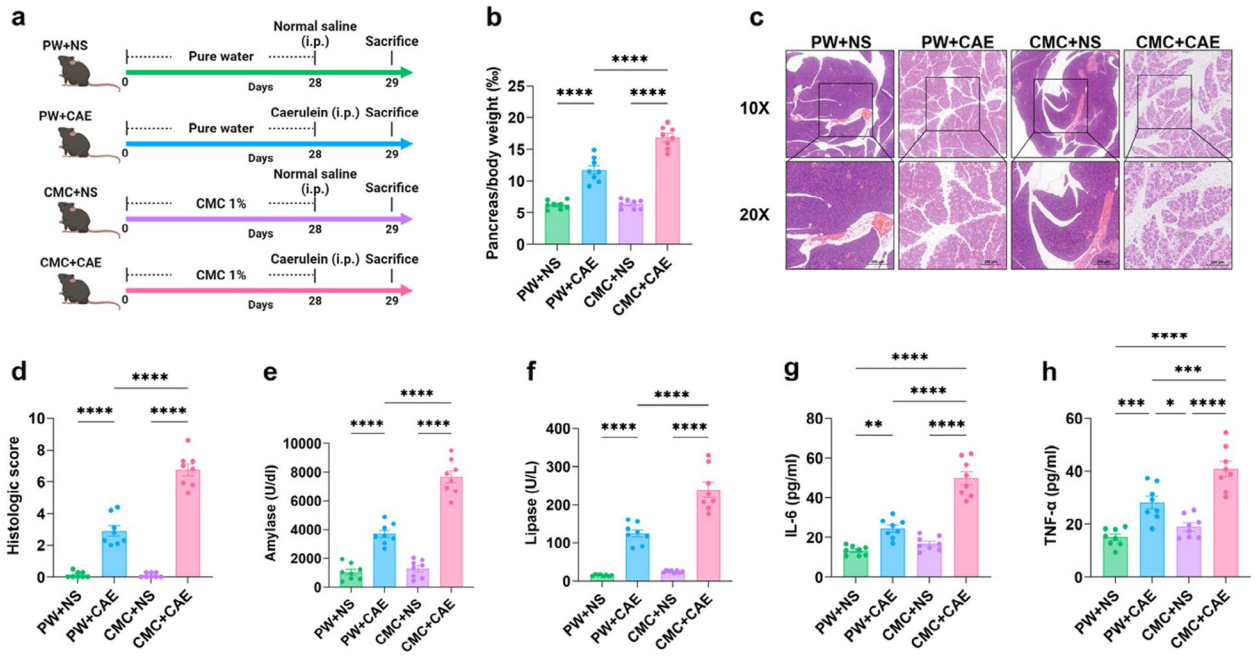


**Fig. 1** CMC exacerbated caerulein-induced AP. **a** Experimental scheme, mice drink pure water (PW) or CMC solution (1%) for the first 28 days, and on the 28th day, after fasting for 8 h, the mice were given intraperitoneal injections of either normal saline (NS) or caerulein (CAE), respectively. **b** Pancreas-to-body weight ratio. **c** Representative images of pancreatic H&E staining. **d** Histologic score. **e** Serum amylase. **f** Serum lipase. **g** Serum IL-6. **h** Serum TNF-α. $n = 8$. *$p < 0.05$, **$p < 0.01$ and ***$p < 0.001$****$p < 0.0001$. CMC, carboxymethylcellulose; AP, acute pancreatitis

### CMC altered gut microbial composition in mice with AP

To explore potential changes in gut microbiota resulting from CMC exposure, we conducted full-length 16S rRNA amplicon sequencing of fecal samples. Notably, alpha diversity significantly decreased in the PW + CAE, CMC + NS, and CMC + CAE groups compared to the PW + NS group (Fig. 2a). We employed principal coordinates analysis (PCoA) to evaluate beta diversity, revealing distinct clustering among the four groups (Fig. 2b). Further examination revealed alterations of gut microbiota at various taxonomic levels. Specifically, at the phylum level, the CMC + CAE group exhibited a significant increase in the relative abundance of Proteobacteria, Campilobactre, and Bacteroidota, along with a marked decrease in Verrucomicrobiota and Deferribacterota compared to the PW + CAE group (Fig. 2c); at the genus level, the CMC + CAE group showed higher relative abundance of several bacteria, including *Escherichia – Shigella*, *Bacteroides*, and *Clostridium_sensu_stricto_1*, while *Akkermansia*, *Muribaculaceae*, and *Lactobacillus* were notably reduced compared to the PW + CAE group (Fig. 2d,e).

To identify the specific bacteria associated with CMC-induced AP exacerbation, we conducted an in-depth analysis of bacterial differences between the PW + CAE group and the CMC + CAE group. Our analysis, including species differences and LEfSe analysis, revealed significantly higher relative abundances of *Escherichia coli*, *Clostridium perfringens*, and *Bacteroides vulgatus* in the CMC + CAE group, whereas *Akkermansia muciniphila*, *Lactobacillus unclassified*, and *Lachnospiraceae bacterium* were markedly reduced (Fig. 2f–h). Additionally, we employed BugBase, a bioinformatics tool for predicting community-wide phenotypes, to assess phenotypic differences among the four groups. Notably, the relative abundance of potentially pathogenic bacteria significantly increased in the CMC + CAE group compared to the PW + CAE group (Fig. 2i). Collectively, these findings indicate that CMC induced alterations in the gut microbiota of mice with AP, leading to an increase in potentially pathogenic bacterial abundance.

### CMC exacerbated AP in a gut microbiota-dependent manner

To investigate if alterations of gut microbiota contribute to CMC's negative impacts on AP, we conducted FMT from PW or CMC-exposed mice into two different sets of mice: antibiotic-treated specific-pathogen-free (SPF) mice (Additional file 1: Fig. S1a) and germ-free (GF) mice (Fig. 3a).

The gut microbiota of recipient mice was profiled after FMT. Beta-diversity analysis showed distinct microbial communities between FMT-Ctrl and FMT-CMC groups (Additional file 1: Fig. S1b), as well as between GF-FMT-Ctrl and GF-FMT-CMC groups (Fig. 3b). Consistent

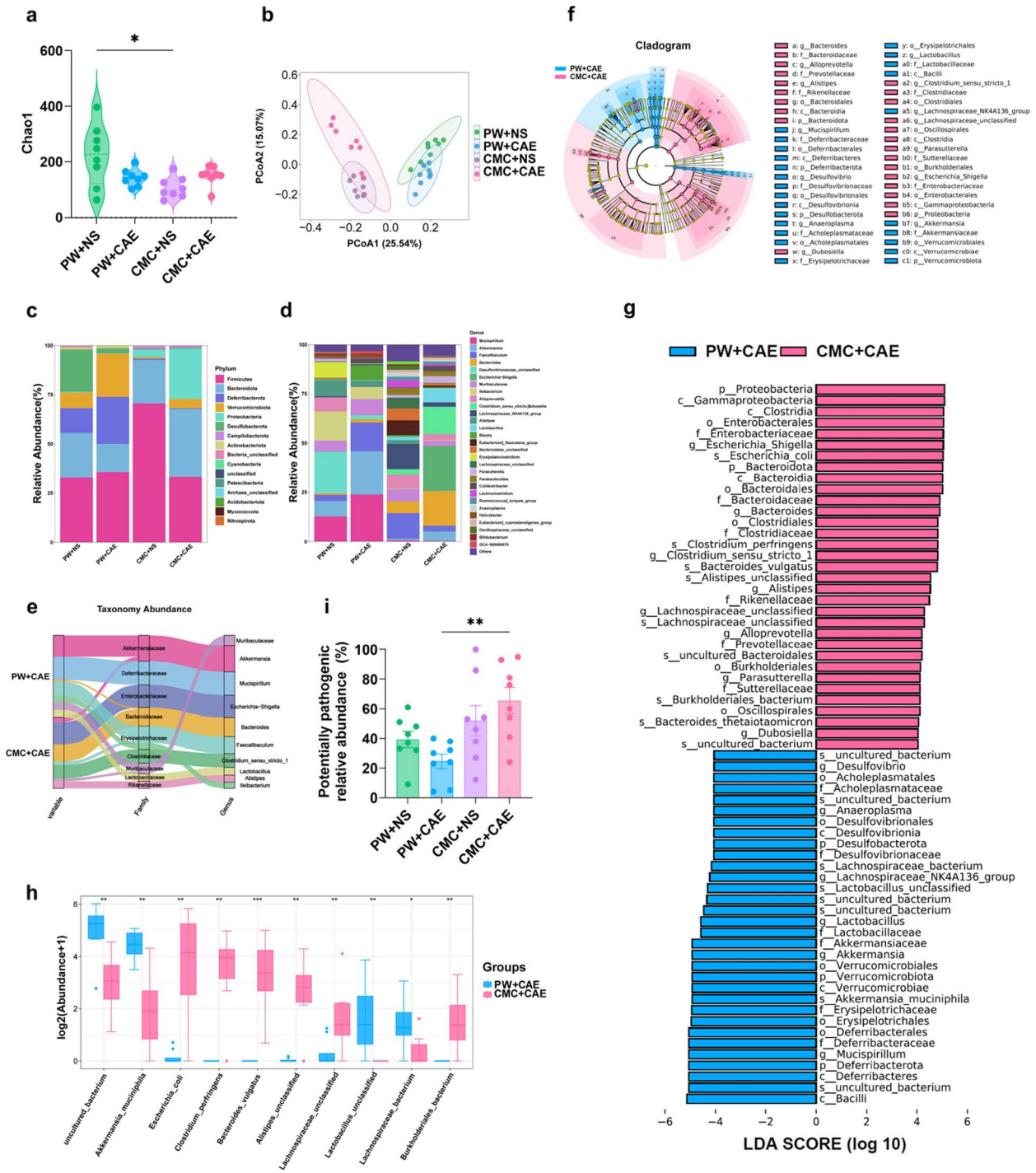


**Fig. 2** CMC altered gut microbiota in mice with AP. **a** Alpha diversity (based on Chao1). **b** PCoA of beta diversity using unweighted unifrac distance. Relative abundance of taxa at the phylum (**c**), and genus (**d**) levels. **e** The Sankey chart presents the family and genus level pattern of change in gut microbiota between the PW + CAE and CMC + CAE groups. **f** Cladograms generated by LEfSe indicating differences in the bacterial taxa between PW + CAE and CMC + CAE group. **g** LDA score for the bacterial taxa differentially abundant between PW + CAE and CMC + CAE groups (LDA > 4.0). **h** Boxplot of difference analysis at species level (Top 10). **i** Relative abundance of those potentially pathogenic bacteria. $n = 8$. *$p < 0.05$, **$p < 0.01$ and ***$p < 0.001$****$p < 0.0001$. CMC, carboxymethylcellulose; AP, acute pancreatitis; PW, pure water; CAE, caerulein; PCoA, principal coordinate analysis; LDA, linear discriminant analysis; LEfSe, linear discriminant analysis effect size

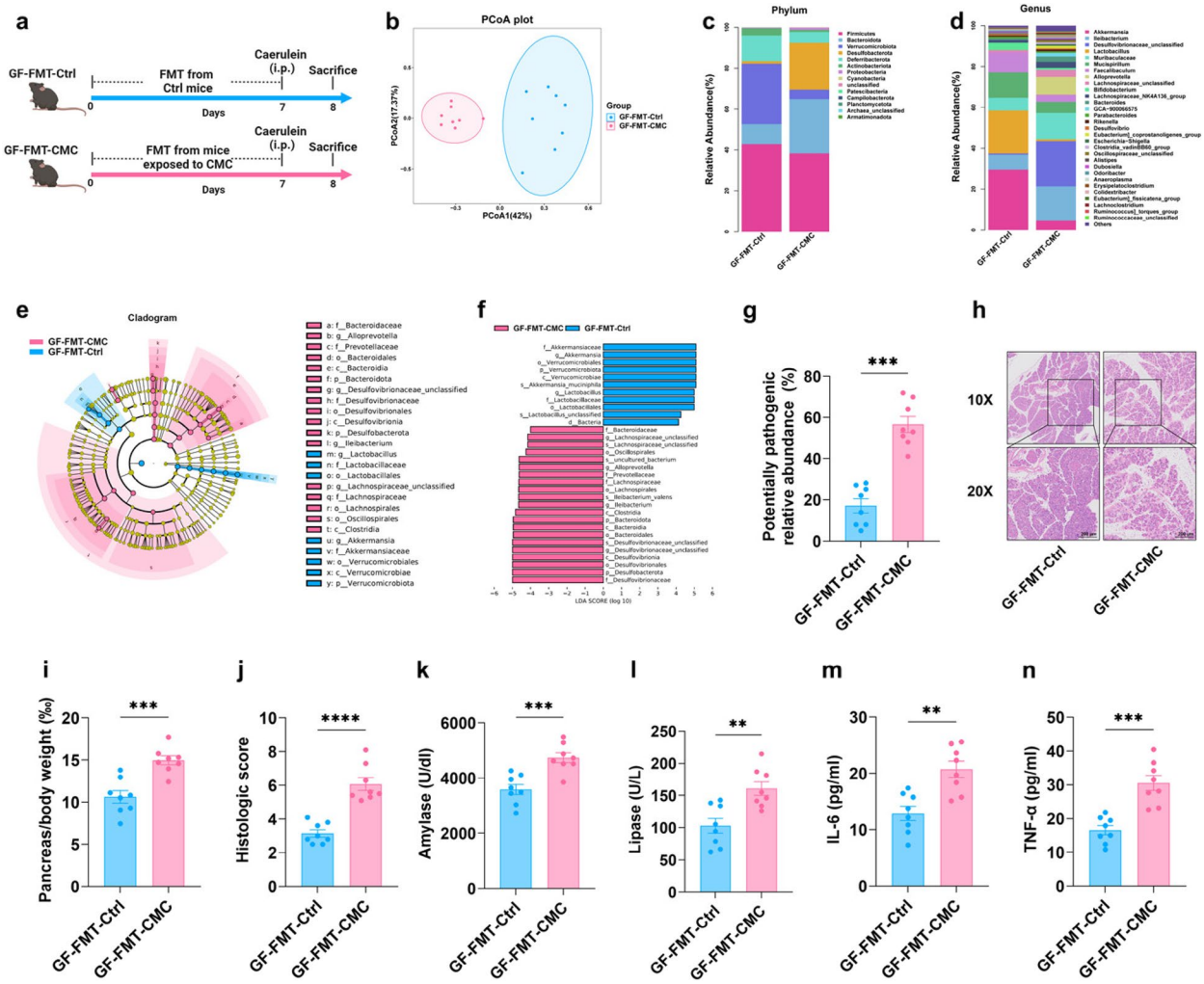


**Fig. 3** FMT from mice exposed to CMC exacerbated AP in GF mice. **a** Schematic diagram of the experimental design using germ-free (GF) mice. Mice in the GF-FMT-Ctrl group received FMT from control mice on the first 7 days, while mice in the GF-FMT-CMC group received FMT from mice exposed to CMC, and on the 7th day, after fasting for 8 h, mice in two groups were given intraperitoneal injections of caerulein (CAE) to induce AP. **b** Principal coordinates analysis (PcoA) plot assessing beta diversity. Relative abundance distribution of bacteria in phylum (**c**) and genus (**d**) level. **e** The cladogram representing the significantly different microbial features between GF-FMT-Ctrl and GF-FMT-CMC groups. **f** Linear discriminant analysis effect size (LEfSe) analysis showing bacterial taxa that were significantly different in abundance between GF-FMT-Ctrl and GF-FMT-CMC groups. **g** Relative abundance of potentially pathogenic bacteria predicted based on the BugBase database. **h** Representative images of pancreatic H&E staining. **i** Pancreas-to-body weight ratio. **j** Histologic score. **k** Serum amylase. **l** Serum lipase. **m** Serum IL-6. **n** Serum TNF-α. $n = 8$. *$p < 0.05$, **$p < 0.01$ and ***$p < 0.001$****$p < 0.0001$. GF mice, germ-free mice; FMT, fecal microbiota transplantation

with microbiota alteration between PW + CAE and CMC + CAE groups, the FMT-CMC/GF-FMT-CMC groups exhibited a significant increase in the relative abundance of Bacteroidota and Desulfobacterota, while Verrucomicrobiota levels markedly decreased at the phylum level; at the genus level, the FMT-CMC/GF-FMT-CMC groups had higher relative abundance of various bacteria, including *Desulfovibrionaceae_unclassified*, *Alloprevotella*, and *Bacteroides*, while *Akkermansia* and *Lactobacillus* were noticeably reduced (Fig. 3c-f, Additional file 1: Fig. S1c–f). Predictions based on the BugBase database showed potentially pathogenic bacteria abundance increased in the FMT-CMC/GF-FMT-CMC groups compared to the FMT-Ctrl/GF-FMT-Ctrl groups (Fig. 3g, Additional file 1: Fig. S1g).

In both experimental models, mice receiving FMT (FMT-CMC/GF-FMT-CMC) from CMC-exposed donors exhibited more severe pancreatic tissue damage, as evidenced by higher pancreas-to-body weight ratio, elevated histologic scores (Fig. 3h–j, Additional file 1: Fig. S1h–j), increased serum levels of amylase, lipase, IL-6, and TNF-α (Fig. 3k–n, Additional file 1: Fig. S1k–n),

compared to those receiving FMT from control donors. FMT from CMC-exposed mice transferred adverse effects to both SPF and GF recipient mice, which demonstrated the crucial role of gut dysbiosis in CMC-induced AP exacerbation.

### scRNA-seq identified classical monocytes as top altered immune cells in FMT-CMC group

Mounting evidence suggests that gut microbiota can influence distant organs by regulating immunity [13, 14]. To further elucidate mechanisms behind CMC-induced AP exacerbation, we employed single-cell RNA sequencing (scRNA-seq) to study the cellular heterogeneity of peripheral blood mononuclear cells (PBMCs) in the FMT-Ctrl and FMT-CMC groups.

Fifteen cell clusters, derived from six major clusters, including monocytes, DCs, T cells, basophils, NK cells, and B cells, were identified (Fig. 4a, Additional file 1: Fig. S2a–d). Cell number for each cluster and sample was displayed to confirm the clustering's accuracy (Fig. 4b). Top markers for each cluster were shown in a heatmap (Fig. 4c). Interestingly, we observed a significantly higher frequency of monocytes in the FMT-CMC group compared to the FMT-Ctrl group ($p=0.017$), with no differences among the other major clusters (Fig. 4d). Specifically, classical monocytes, which are known for their pro-inflammatory roles in AP [15], exhibited significant differences between the two groups (Fig. 4e).

Gene set variation analysis (GSVA) and transcriptional regulon analysis indicated that classical/intermediate monocytes displayed more pro-inflammatory features than Non-classical monocytes (Additional file 1: Fig. S3a, c). GSEA analysis for classical monocytes reported upregulation of cell communication (NES = 1.82), cytokine production (NES = 1.89), and immune system process pathways (NES = 2.06) in the FMT-CMC group (Additional file 1: Fig. S3b). Pro-inflammatory pathways were significantly upregulated in FMT-CMC group cells compared to FMT-Ctrl group cells, including cellular response to interleukin-1 (NES = 2.08), inflammatory response (NES = 2.07), and myeloid leukocyte migration pathways (NES = 1.93) (Fig. 4f). PROGENy analysis also revealed enrichment of JAK-STAT, NFκB, and TNFα pathways in FMT-CMC group cells (Fig. 4g).

Next, we used Monocle 2 to infer the developmental trajectory of classical monocytes, dividing them into five states (S1-S5) along pseudotime (Fig. 4h). Classical monocytes from the FMT-CMC group were predominantly enriched in S4 and S5, representing relatively late pseudotime states (Fig. 4h). Transcriptional analysis revealed two distinct gene sets associated with inflammatory roles in classical monocytes (Fig. 4i). Cell–cell communication analysis highlighted significant factors between classical monocytes and other cells (Fig. 4j). These findings suggest that FMT from CMC-exposed mice increases classical monocytes in recipient mice peripheral blood, potentially contributing to CMC-induced AP exacerbation.

### Analysis of upstream regulators revealed that LPS-stimulated C/EBPδ drives monocytes towards classical phenotype

Regulon activity was calculated to assess upstream regulons driving the heterogeneity of monocytes. We found that CCAAT/enhancer-binding protein delta (C/EBPδ) was the most specific regulon associated with classical monocytes based on RNA profiles (Fig. 5a). Meanwhile, the expression level of C/EBPδ in classical monocytes surpasses that in all other cell types within PBMCs (Fig. 5b). UMAP plot provides additional support that the activity of C/EBPδ was highly specific to classical monocytes (Additional file 1: Fig. S4a). To determine the effect of C/EBPδ expression on monocytes polarization, we transfected RAW264.7 cell with pC/EBPδ or siC/EBPδ for 48 h. Transfection efficacy was validated by quantitative reverse-transcription PCR (qRT-PCR) (Fig. 5c). We found that overexpression of C/EBPδ in RAW264.7 cell resulted in significant increase of levels of classical monocytes markers, e.g., S100a8, S100a9, Lcn2, Cxcl2, and Ifitm1, whereas knockdown of C/EBPδ did the

(See figure on next page.)

**Fig. 4** scRNA-seq identified classical monocytes as top altered immune cells in mice received FMT from mice exposed to CMC. **a** Uniform Manifold Approximation and Projection plot: 15 cell types identified by scRNA-seq. **b** Cell number and composition of different cell types in FMT-Ctrl and FMT-CMC group. **c** The top DEGs of each major cell type. The red color in the heatmap means highly expressed genes. **d** The cell composition differences between the FMT-Ctrl and FMT-CMC groups for each major cell cluster-monocytes, Dcs, T cells, basophils, Nk cells, and B cells. Ns, not significant. **e** The cell composition differences between FMT-Ctrl and FMT-CMC groups for each monocyte subgroup. ns, not significant. **f** Gene weight rank for FMT-CMC VS FMT-Ctrl samples in scRNA-seq data by GSEA analysis. Different colors of curves represent the significant pathways. **g** GSVA result heatmap for pathways activity in FMT-Ctrl and FMT-CMC group by progeny. Scaled, red for highly enriched, blue for lowly enriched. **h** Trajectory feature plots for classical monocytes in pseudotime analysis. The S1–S5 five directions have different cell compositions. The bright color represents the late stage. **i** DEGs in the early and late stages during pseudotime. Scaled, red for highly expressed, blue for lowly expressed. The horizon axis represents the stage from early to late. **j** Bubble plot for cell–cell interaction level between Mono_classical cells and other cells, only shows the significant interactions in CellphoneDB ($p<0.05$). Scaled, red for highly interacted, blue for lowly interacted. $n=4$

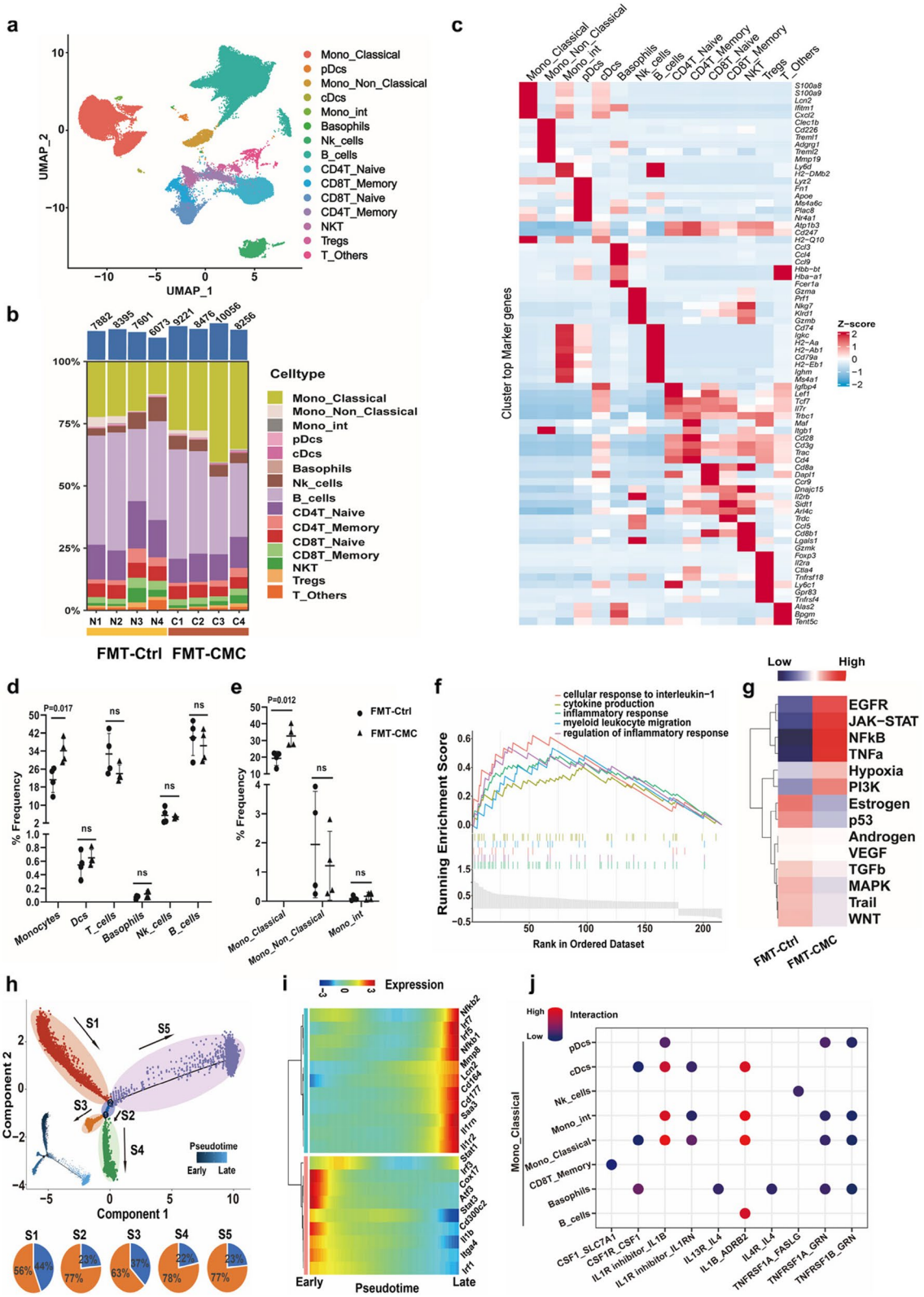


**Fig. 4** (See legend on previous page.)

opposite, demonstrating that C/EBPδ plays a critical role in polarization of monocytes towards pro-inflammatory (classical) phenotype (Fig. 5c).

To investigate the role of monocytes C/EBPδ in the process of CMC worsening AP. We conducted a monocyte-specific C/EBPδ knockdown mouse experiment. On the first day, Cx3cr1-iCre Cas9-KI mice were injected intravenously with AAV-DIO-shRNA (C/EBPδ) or AAV-DIO-shRNA (NC) based on their group assignment, and then they were provided with pure water or CMC solution (1%) to drink, depending on their group, for a 28-day intervention period. On day 28, AP was induced in all four groups using caerulein (Fig. 5d, e). qPCR results demonstrate that we successfully achieved a specific knockdown of C/EBPδ in mouse monocytes (Additional file 1: Fig. S4b). Compared to the AAV-DIO-shRNA(NC)+CMC group, mice in the AAV-DIO-shRNA(C/EBPδ)+CMC group showed significant alleviation of AP, characterized by lower histological scores (Fig. 5f,g), pancreatic/body weight (Additional file 1: Fig. S4c), serum amylase, serum lipase, serum IL-6, and serum TNF-α levels (Additional file 1: Fig. S4d–g). Additionally, the proportion of classical monocytes in the PBMCs of the AAV-DIO-shRNA(C/EBPδ)+CMC group was reduced compared to the AAV-DIO-shRNA(NC)+CMC group (Fig. 5h, Additional file 1: Fig. S4h), as illustrated in the gating strategy shown in Additional file 1: Fig. S4i. Our results demonstrate that monocyte-specific C/EBPδ knockdown can reverse the increase in the proportion of classical monocytes caused by CMC, alleviate the exacerbation of AP induced by CMC.

We further investigated the potential factor contributing to upregulation of C/EBPδ. GSEA analysis showed that the inflammatory response lps up (NES=1.79) pathway was among the most significantly enriched pathways in the FMT-CMC group (Fig. 5i). Serum LBP (lipopolysaccharide-binding protein) levels were measured as an indirect indicator of LPS levels. Quantification of serum LBP further confirmed its elevated profile in both the CMC exposure group and recipient mice that received feces from CMC-exposed mice. (Fig. 5j, k; Additional file 1: Fig. S5a), aligning with its established role as a C/EBPδ activator in previous studies [16]. In vitro analysis demonstrated that LPS stimulation induced a noticeable increase in the expression levels of C/EBPδ and classical monocytes markers in RAW264.7 cells, conversely, knockdown of C/EBPδ attenuated these effects (Fig. 5l). These findings collectively demonstrate the causal relationship between LPS and C/EBPδ activation, as well as classical monocytes polarization.

Given that elevated serum LPS is usually associated with increased intestinal permeability, we further investigated the impact of CMC on gut barrier function in AP mice. Levels of tight junction proteins in the gut epithelium, including Zonula occludens-1 (ZO-1) and claudin-1, were significantly decreased following direct or indirect (via FMT) exposure to CMC (Additional file 1: Fig. S6a–l). These findings indicate that CMC exposure led to the impairment of the gut barrier, resulting in increased serum LPS levels in AP mice.

We further conducted a rescue experiment utilizing eritoran, a competitive antagonist of LPS (Fig. 5m), to assess the contribution of elevated serum LPS to CMC-induced AP aggravation. Intraperitoneal injection of eritoran in CMC-exposed AP mice resulted in a reduction of histologic score (Fig. 5n, o) and pancreas-to-body weight ratio (Additional file 1: Fig. S5b), along with decreased serum

(See figure on next page.)

**Fig. 5** C/EBPδ induced by LPS is a key transcriptional factor for classical monocyte activation. **a** Regulons activity ranks in classical monocytes. **b** Violin plots indicating the C/EBPδ expression levels in different cell types of PBMCs. **c** The relative expression of classical monocyte markers in control and C/EBPδ-overexpressed RAW264.7 cells, analyzed by qRT-PCR. The mRNA expression levels of each gene were normalized to fold over β-actin (housekeeping gene) ($n=3$). **d** The diagram of monocytes C/EBPδ knockdown mice preparation. AAV-DIO-shRNA (C/EBPδ) or AAV-DIO-shRNA (NC) was injected into Cx3cr1-iCre Cas9-KI mice' tail vein. **e** Monocyte-specific C/EBPδ knockdown mouse experiment. On the first day, Cx3cr1-iCre Cas9-KI mice were injected intravenously with AAV-DIO-shRNA (C/EBPδ) or AAV-DIO-shRNA (NC) based on their group assignment, and then they were provided with pure water or CMC solution (1%) to drink, depending on their group, for a 28-day intervention period. On day 28, AP was induced in all four groups using caerulein. **f** Representative images of pancreatic H&E staining. **g** Histologic score. **h** Flow cytometry (FCM) analysis showed proportions of classical monocytes in PBMC of mice ($n=3$). **i** Gene weight rank for FMT-CMC monocytes VS FMT-Ctrl monocytes in scRNA-seq data by GSEA analysis. Different colors of curves represent the significant pathways. **j** Serum LBP of FMT-Ctrl and FMT-CMC groups ($n=8$). **k** Serum LBP of PW+NS, PW+CAE, CMC+NS, and CMC+CAE groups ($n=8$). **l** The relative expression of classical monocyte markers in RAW264.7 cells treated with blank, LPS (10 ng/ml), LPS (10ng/ml)+sh-C/EBPδ, analyzed by qRT-PCR. The mRNA expression levels of each gene were normalized to fold over β-actin (housekeeping gene) ($n=3$). **m** Eritoran rescue experiment design ($n=8$). In Ctrl and Ctrl+Eritoran groups, mice took pure water for 28 days, and on day 28, the Ctrl group received an intraperitoneal injection of NS, while the Ctrl+Eritoran group received an intraperitoneal injection of Eritoran. In CMC and CMC+Eritoran groups, mice took CMC solution (1%) for 28 days. On day 28, the CMC group received an intraperitoneal injection of NS, while the CMC+Eritoran group received an intraperitoneal injection of Eritoran. One hour after the injection of NS or Eritoran, AP was induced in all four groups using caerulein. **n** Representative images of pancreatic H&E staining. **o** Histologic score. **p** Flow cytometry (FCM) analysis showed proportions of classical monocytes in PBMC of mice ($n=4$). *$p<0.05$, **$p<0.01$ and ***$p<0.001$ ****$p<0.0001$. AP, acute pancreatitis; LBP, lipopolysaccharide-binding protein; PBMCs, peripheral blood mononuclear cells

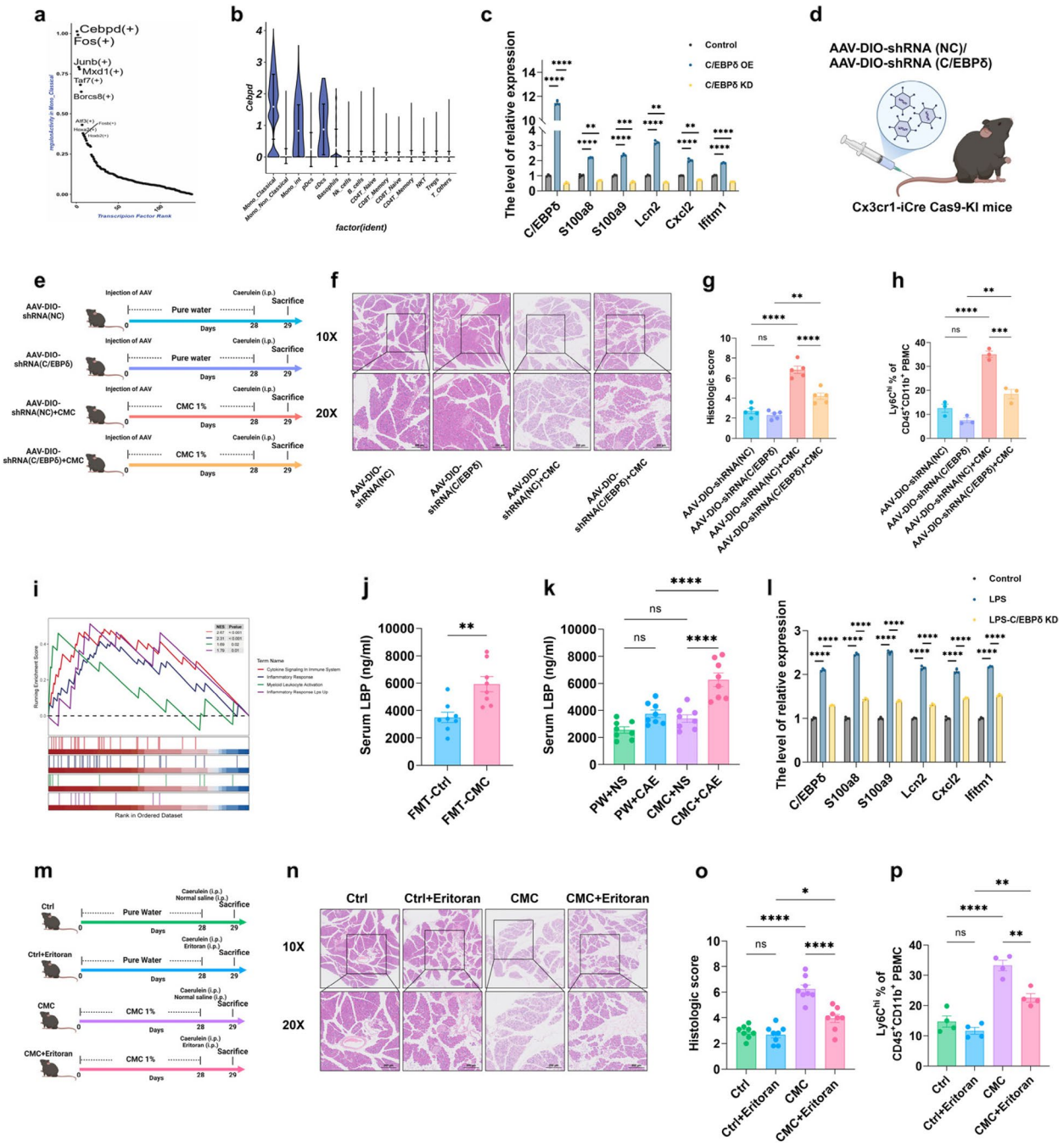


**Fig. 5** (See legend on previous page.)

levels of amylase, lipase, IL-6, and TNF-α (Additional file 1: Fig. S5c–f). Consistently, the frequency of classical monocytes in PBMCs decreased in the CMC + Eritoran group compared to the CMC group (Fig. 5p, Additional file 1: Fig. S5g). Collectively, these data indicate that C/EBPδ-driven classical monocyte activation, induced by impaired gut barrier and subsequent LPS leakage, plays a crucial role in mediating the promotive effects of CMC on AP.

### Butyrate supplementation ameliorates AP exacerbation induced by CMC

Since SCFAs protect gut barrier integrity through nourishing intestinal epithelial cells [17], we quantified SCFA levels in the feces of mice. Compared to PW + CAE, CMC + CAE showed decreased propionate, butyrate, and total SCFA concentrations (Fig. 6a–d). Furthermore, total SCFAs, acetate, propionate, and butyrate, in the feces of

he FMT-CMC/GF-FMT-CMC group were significantly lower compared to FMT-Ctrl/GF-FMT-Ctrl group (Additional file 1: Fig. S7a–h). To identify the specific subtype of SCFAs responsible for CMC-induced AP exacerbation and gut barrier impairment, we did correlation analysis and found that butyrate exhibited the most potent correlation with AP severity parameters (Fig. 6e). Then we conducted a rescue experiment to validate butyrate's potential effects in mitigating AP severity (Fig. 6f). Fecal butyrate deletion due to CMC exposure were reversed by butyrate gavage (Fig. 6g).

Butyrate supplementation significantly ameliorates CMC's detrimental effects on AP, with reduced levels of a list of AP severity parameters, e.g., pancreas-to-body weight ratio, histologic score (Fig. 6h-j), serum amylase, lipase, IL-6, TNF-α (Additional file 1: Fig. S7i–l). Moreover, gut barrier function was partially restored, with increased levels of ZO-1 and claudin-1 (Fig. 6k, l; Additional file 1: Fig. S7m, n), and decreased serum LBP level (Fig. 6m). Classical monocyte frequency in PBMCs was also decreased (Fig. 6n; Additional file 1: Fig. S7o). These results suggest that butyrate depletion plays a role in the adverse effects of CMC on AP, and supplementation with butyrate mitigates these effects.

### *Akkermansia muciniphila* supplementation ameliorates AP exacerbation induced by CMC

We employed correlation matrices to further identify specific gut bacteria that relate to the detrimental effects of CMC. Among the five significantly altered bacteria strains, including *Akkermansia muciniphila*, *Escherichia coli*, *Clostridium perfringens*, *Bacteroides vulgatus*, *Alistipes unclassified*, and *Akkermansia muciniphila* exhibited the strongest correlation with AP severity. A diminished abundance of *Akkermansia muciniphila* was associated with elevated serum LPS, IL-6, TNF-α, pancreas-to-body weight ratio, and pancreatic histologic score, as well as lowered gut barrier makers (ZO-1, claudin-1) and fecal SCFAs levels (Fig. 7a), which are in line with *Akkermansia muciniphila*'s established role as a crucial beneficial probiotic that fortifies the gut barrier [18].

We further conducted a rescue experiment to validate *Akkermansia muciniphila*'s potential effects in mitigating AP severity (Fig. 7b). Administration of *Akkermansia muciniphila* through gavage significantly increased its relative abundance in CMC + AKK group (Fig. 7c). This led to a reduction in pancreas-to-body weight ratio and histologic score (Fig. 7d–f), decreased serum amylase, lipase, IL-6, and TNF-α (Additional file 1: Fig. S8a–d), restored gut barrier function (Fig. 7g–i, Additional file 1: Fig. S8e, f) and elevated fecal SCFAs (Additional file 1: Fig. S8g–j), as compared with CMC group. Classical monocyte levels in PBMCs concordantly decreased in the CMC + AKK group compared to the CMC group (Fig. 7j; Additional file 1: Fig. S8k). In summary, *Akkermansia muciniphila* supplementation alleviated AP, reinforced gut barrier, and elevated fecal SCFAs in the context of CMC exposure.

We further performed a correlation analysis between *Akkermansia muciniphila* abundance and AP severity in humans. The gut microbiota of 54 AP patients were assessed using full-length 16S rRNA sequencing (Fig. 7k). Compared with mild AP (MAP) group, moderately severe or severe (MSAP/SAP) group showed lower alpha diversity (Additional file 1: Fig. S9a). PCoA was used to assess the β-diversity based on bray–curtis (ANOSIM $R = 0.0444$, $p = 0.088$) distances between the MSAP/SAP and MAP groups (Additional file 1: Fig. S9b). At the phylum level, the relative abundance of Proteobacteria was significantly increased, while Verrucomicrobiota abundance was drastically decreased in MSAP/SAP group compared with that in MAP group (Additional file 1: Fig. S9c); at the genus level, the relative abundance of *Escherichia – Shigella* was higher, whereas *Akkermansia*, *Muribaculaceae*, and *Ruminococcaceae* were noticeably decreased in MSAP/SAP group compared with that in MAP group (Additional file 1: Fig. S9d, e). Differential analysis of species level suggests that *Escherichia coli* abundance was increased while *Akkermansia muciniphila* was decreased in MSAP/SAP group compared with that in MAP group (Fig. 7l). Moreover, *Akkermansia muciniphila* abundance showed a negative correlation with the bedside index for severity in AP (BISAP) score [8] (Fig. 7m) and C-reactive protein (CRP) (Fig. 7o). Based on the presence or absence of Systemic Inflammatory Response Syndrome (SIRS) in AP, the cases were

(See figure on next page.)

**Fig. 6** Butyrate relieved AP aggravated by CMC. Fecal total SCFAs (**a**), acetate (**b**), propionate (**c**), and butyrate (**d**) concentration ($n = 8$). **e** Correlation analysis between feces SCFAs and AP phenotype and gut barrier function identifies the contributing feces metabolite. **f** Butyrate rescue experiment design ($n = 8$). In the Ctrl group, mice took pure water for 28 days, on days 14–28 supplementing water gavage. In the CMC and CMC + Butyrate groups, mice took CMC solution (1%) for 28 days, on days 14–28, supplementing water gavage for the CMC group and butyrate solution gavage for the CMC + Butyrate group. **g** Fecal butyrate concentration. **h** Pancreas-to-body weight ratio. **i** histologic score. **j** Representative images of pancreatic H&E staining. The gut barrier function of mice was evaluated and compared by western blot (**k**) and immunofluorescence (**l**) of ZO-1 and claudin-1 protein. **m** Serum LBP level. **n** Flow cytometry (FCM) analysis showed proportions of classical monocytes in PBMCs of mice ($n = 4$). *$p < 0.05$, **$p < 0.01$ and ***$p < 0.001$ ****$p < 0.0001$. LBP, lipopolysaccharide-binding protein; PBMCs, peripheral blood mononuclear cells

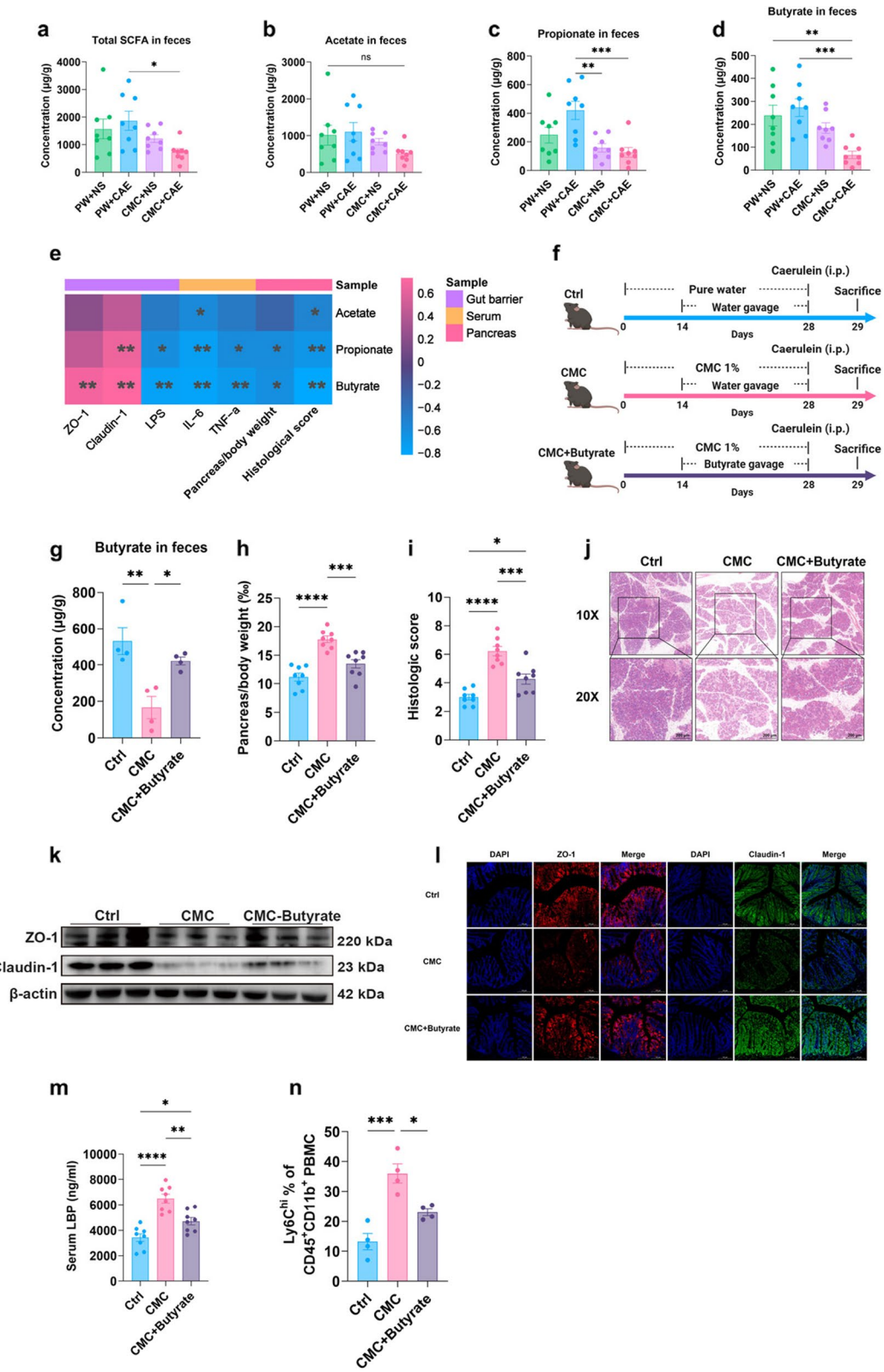


**Fig. 6** (See legend on previous page.)

divided into SIRS and non-SIRS groups, compared to the non-SIRS group, the abundance of AKK was significantly reduced in the SIRS group (Additional file 1: Fig. S9f). These findings suggest that diminished gut *Akkermansia muciniphila* may be a potential indicator for severe AP (Fig. 8).

## Discussion

Though various studies showed that environmental factors, e.g., the Western diet, contribute a lot to the annual increase of AP incidence, no previous research reported the role of those ubiquitous food additives in AP pathogenesis. The current study demonstrated for the first time that one common food additive, CMC, worsens AP, which is accompanied with gut dysbiosis. Through FMT from CMC-exposed mice to SPF or GF mice, an exaggerated AP phenotype was transferred, suggesting that altered gut microbiota mediates CMC's adverse effects on AP. Single-cell sequencing identified classical monocytes as potential key effector cells in mediating AP promotion by CMC. CMC exposure led to reduced fecal SCFAs, especially butyrate, contributing to increased intestinal permeability and exacerbating AP by allowing LPS into the bloodstream. Mechanistically, elevated serum LPS upregulated C/EBPδ in monocytes, promoting the activation of classical monocytes, thereby exacerbating AP. This gut microbial shift is featured with increased pathogenic bacteria and reduced probiotics, with *Akkermansia muciniphila* showing the strongest correlation with AP severity. Supplementation with *Akkermansia muciniphila* or butyrate mitigated CMC-induced AP exacerbation.

Numerous studies highlighted CMC's detrimental impacts on human health by disrupting gut microbiota [4, 5], which induces low-grade inflammation and promotes the development of chronic diseases. However, no research to date has explored the potential impact of CMC on acute inflammatory diseases. AP is a pancreatic disorder triggered by damage to acinar cells, leading to both local and systemic inflammations. The degree of systemic inflammation in AP varies, with potential complications and life-threatening conditions in certain cases. Multiple evidence supports the potential pathogenic role for gut dysbiosis in AP. For example, gut microbiota differs both between AP patients and healthy volunteers [19] and among AP patients with different severity grades [20]. Depleting the gut microbiota using antibiotics alleviates AP in mice [21]. All these findings drive us to explore if CMC could regulate AP through modulating gut microbiota. Our data showed that CMC exposure significantly altered gut microbiota in the setting of AP, reducing α-diversity and increasing potential pathogenic bacteria. Concurrently, certain probiotics, including *Akkermansia muciniphila* and *Lactobacillus unclassified*, decreased. FMT from CMC-exposed mice to GF and antibiotics-treated SPF mice successfully transferred the AP-promotive phenotype, indicating that gut microbiota mediates the adverse effects of CMC on AP.

We further explored the molecular mechanism underlying CMC's negative effects on AP. Since exaggerated AP is characterized with enforced systemic inflammation, we hypothesized if certain immune cell types in circulation mediate the detrimental impacts of CMC. We conducted scRNA-seq analysis on PBMCs from FMT-Ctrl and FMT-CMC groups. Among the six major cell clusters (monocytes, DCs, T cells, basophils, NK cells, and B cells), only the frequency of monocytes was significantly increased in the FMT-CMC group. Further analysis revealed a marked increase in the classical subtype (Ly6C+), a well-known inflammation-initiator monocyte type, with the ability to differentiate into macrophages within tissues [22]. This aligns with their pro-inflammatory role during the AP process [15], indicating their involvement in classical monocytes' promotive effects on AP. Regulons activity analysis revealed that C/EBPδ stands out as the most specific regulon associated with classical monocytes. Enforced expression of C/EBPδ in RAW264.7 cells significantly upregulated those marker genes for classical

(See figure on next page.)

**Fig. 7** *Akkermansia muciniphila* alleviating AP aggravated by CMC. **a** Correlation analysis between gut bacteria abundance and disease phenotype identifies the contributing gut bacterium on pancreatitis phenotype and gut barrier function. **b** *Akkermansia muciniphila* rescue experiment design ($n=8$). In the Ctrl group, mice took pure water for 28 days, on days 14–28 supplementing PBS gavage. In the CMC and CMC + AKK groups, mice took CMC solution (1%) for 28 days, on days 14–28, supplementing PBS gavage for the CMC group and *Akkermansia muciniphila* gavage for the CMC + AKK group. **c** *Akkermansia muciniphila* abundance by qRT-PCR. **d** Pancreas-to-body weight ratio. **e** Histologic score. **f** Representative images of pancreatic H&E staining. Gut barrier function of mice was evaluated and compared by western blot (**g**) and immunofluorescence (**h**) of ZO-1 and claudin-1 protein. **i** Serum LBP level. **j** Flow cytometry (FCM) analysis showed proportions of classical monocytes in PBMCs of mice ($n=4$). **k** Schematic protocal. **l** Boxplot of difference analysis at the species level (Top 5). **m** The correlation between *Akkermansia muciniphila* abundance and the BISAP score of AP patients was analyzed using Spearman's correlation. **o** The correlation between *Akkermansia muciniphila* abundance and CRP level of AP patients was analyzed using Spearman's correlation. *$p<0.05$, **$p<0.01$ and ***$p<0.001$ ****$p<0.0001$. LBP, lipopolysaccharide-binding protein; PBMCs, peripheral blood mononuclear cells. AKK, *Akkermansia muciniphila*

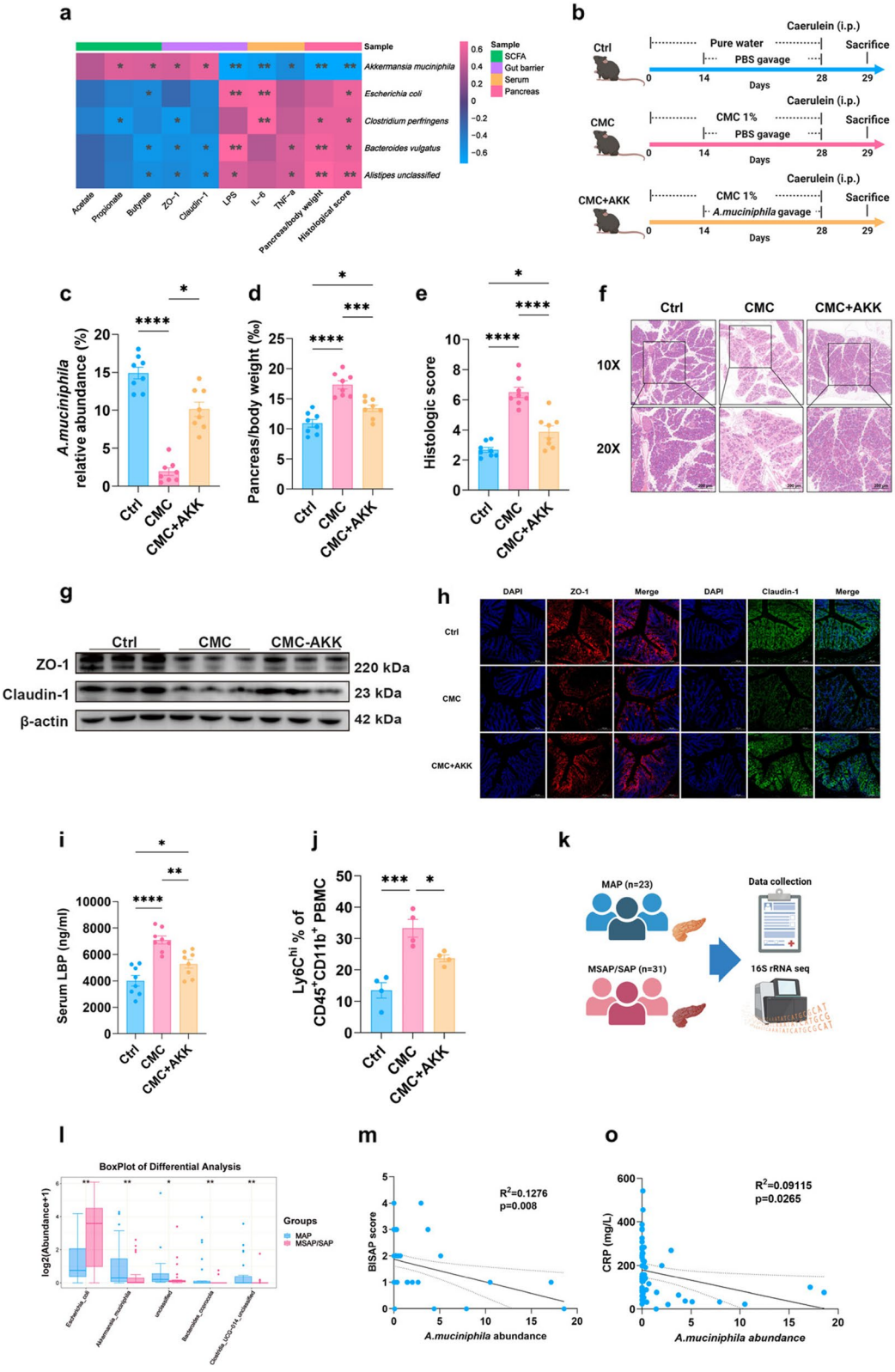


**Fig. 7** (See legend on previous page.)

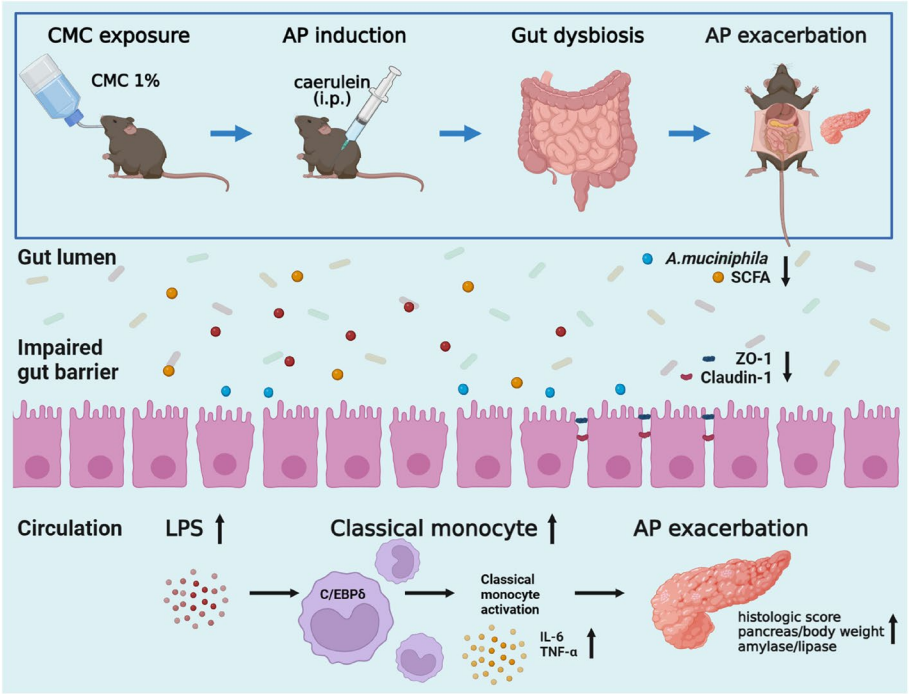


**Fig. 8** Mechanism diagram

monocytes, while knockdown of C/EBPδ did the opposite, emphasizing its critical role in classical monocyte activation. Further, we conducted an experiment involving monocyte-specific knockdown of C/EBPδ in mice. This targeted knockdown was found to reverse the CMC-induced increase in the proportion of classical monocytes and alleviate the exacerbation of acute pancreatitis (AP) caused by CMC. In summary, these studies demonstrate the critical role of C/EBPδ in the CMC-aggravated AP process.

We further employed GSEA analysis to identify the upstream factor contributing to C/EBPδ upregulation. In the FMT-CMC group, the signaling pathway regarding LPS, a known stimulator on C/EBPδ [23], was significantly enriched, aligning with its elevated profile in serum, as compared to the FMT-Ctrl group. Intraperitoneal administration of eritoran, an LPS antagonist [24], successfully alleviated CMC-induced AP exacerbation, with classical monocyte frequency significantly reduced, which highlights the pivotal role of LPS in mediating the detrimental effects of CMC on AP. Gut barrier function analysis showed significantly increased intestinal permeability, as evidenced by diminished expressions of ZO-1 and Claudin-1, which contributed to elevated serum LPS levels. Mechanistically, CMC exposure increases gut permeability, facilitates translocation of LPS into bloodstream, thereby upregulates C/EBPδ, which activates classical monocytes and finally results in AP exaggeration.

UPFs, including those food additives, are endemic in our modern societies, making it difficult for many people to shift towards less processed diets with reduced food additives within the current food systems in a short time. We investigated if certain elements can help counteract the deleterious impacts of CMC against AP. We conducted a correlation analysis to pinpoint specific microbes and metabolites associated with the CMC's promotion of AP. Five bacteria (*Akkermansia muciniphila*, *Escherichia coli*, *Clostridium perfringens*, *Bacteroides vulgatus*, *Alistipes unclassified*) and three major SCFAs (acetate, propionate, butyrate) with most significantly altered profiles were selected as the candidates. Notably, both *Akkermansia muciniphila* and butyrate exhibited strong correlations with various AP severity and gut barrier function parameters, indicating their potential involvement in CMC-related AP exacerbation. Supplementation with *Akkermansia muciniphila* or butyrate alleviated CMC-induced AP aggravation. Interestingly, *Akkermansia muciniphila* supplementation notably restored SCFA levels, especially propionate and butyrate, consistent with its role as an SCFA producer, revealing that diminished *Akkermansia*

*muciniphila* contributes to the reduced butyrate levels after CMC exposure. Further, we detected the gut microbiota in patients with pancreatitis and found a negative correlation between the abundance of Akkermansia muciniphila and the severity of pancreatitis. We acknowledge that our data have limitations. Our AP patient cohort primarily consisted of individuals with biliary pancreatitis, this predominance may introduce bias, as gut microbiome and barrier function can vary with different AP etiologies. Thus, we must be cautious in extending our results to the broader spectrum of AP etiologies.

There remains controversy regarding whether probiotics prophylaxis can help reduce AP severity. From a positive perspective, evidence from preclinical studies suggests that probiotics could stabilize the intestinal barrier and minimize bacterial translocation, thus preventing infection in AP [25]. Clinical trials have documented the benefits of probiotics in some critically ill patients [26]. However, the results of the PROPATRIA trial showed negative outcomes [27]. In patients with predicted severe AP, probiotic prophylaxis did not reduce the risk of infectious complications and was associated with an increased risk of mortality [27]. As of now, probiotics use is rarely recommended in clinical practice guidelines [26]. Significant heterogeneity among different trials is attributed to the type, dose, and timing of probiotic treatment [28]. In this study, we identified that the administration of *Akkermansia muciniphila* can help alleviate AP, providing novel targets for the development of interventional strategies to mitigate the adverse effects of CMC on AP.

## Conclusions

In conclusion, our research demonstrated for the first time that CMC exposure aggravates AP in mouse model, which is dependent on altered gut microbiota. Depletion of probiotics like *Akkermansia muciniphila* results in reduced SCFAs, compromised gut barrier, and LPS leakage, leading to classical monocyte activation and exacerbation of AP. Although our study has limitations, such as lacking of clinical correlation data between CMC exposure and AP, ignorance of other potential probiotics besides *Akkermansia muciniphila* with protective effects against CMC, absence of substantial therapeutic effectiveness of *Akkermansia muciniphila* and butyrate on AP in clinic, our research still has certain significance: given the extensive use of CMC in processed foods, our research unveiled a significant risk factor contributing to the increasing incidence of AP in recent years; moreover, our study has direct translational implications for those patients who exposed to CMC in daily diet, suggesting that supplementing with *Akkermansia muciniphila* or butyrate could potentially prevent AP attacks or alleviate their severity.

## Methods

### Animals

All experimental procedures and mouse care were approved by the Shanghai Changhai Hospital Ethics Committee. Six-week-old male C57BL/6 mice were purchased from GemPharmatech Co., Ltd. (Jiangsu, China) and kept under specific pathogen-free conditions on a 12-h light–dark cycle at a temperature of 20 °C and 40–60% humidity, with free access to water. Mice were exposed to carboxymethylcellulose (CMC) (Sigma, Cat. No. C4888) diluted in the drinking water (1.0% w/v). The same water was used for the pure water-treated (PW) group. These solutions were changed every 3 days. At the beginning of the experiment, 32 mice were randomly divided into four groups: (1) PW + NS; (2) PW + CAE, acute pancreatitis (AP) induction at day 28; (3) CMC + NS; (4) CMC + CAE, $n = 8$ for each group, AP induction at day 28. All mice were kept in autoclaved cages with three to five mice per cage; cages were cleaned once a week.

### Caerulein (CAE)-induced AP

Mice were fasted for 8 h and were then injected with normal saline/caerulein (intraperitoneally, 100 μg/kg body weight, 8 times at 1-h intervals) (ApexBio Technology, Cat. No. B8465, TX, USA) depending on grouping. Mice were sacrificed 24 h after the first injection. Pancreatic tissue was isolated and weighed. The blood, feces, and colon were collected for further measurements.

### Histopathology

For histological analysis, pancreatic tissue was fixed in 10% neutral-buffered formalin, paraffin-embedded, and processed. A 5-μm section was stained with H&E and semiquantitatively scored according to Schmidt's criteria (Table S1) by two board-certified veterinary pathologists in a blinded manner. The final score is calculated by averaging these two values.

### Serum amylase and lipase quantifications

The blood was centrifuged (2000 rpm) for 10 min after standing at room temperature for 0.5 h. Supernatants were collected to obtain serum. Serum was used to detect amylase (Nanjing Jiancheng Bioengineering Institute, Cat. No. C016-1–1) and lipase (Nanjing Jiancheng Bioengineering Institute, Cat. No. A054-2–1) levels according to the manufacturer's instructions.

#### Quantification of cytokine levels

The serum TNF-α (Anogen, Cat. No. MEC1003) and IL-6 (Anogen, Cat. No. MEC1012) levels were measured by ELISA kits according to the manufacturer's instructions.

#### Full-length 16S ribosomal DNA (rDNA) sequencing

Fecal genomic DNA from different samples was extracted using the CTAB according to the manufacturer's instructions. The full-length 16S rRNA gene was amplified using primers 27F: 5′-AGRGTTTGATYNTGGCTCAG-3′ and 1492R: 5′-TASGGHTACCTTGTTASGACTT-3′, which were tagged with specific barcode per sample. PCR amplification was performed in a total volume of 20 μL reaction mixture containing 4 μL of 5 × FastPfu buffer, 2 μL of 2.5 mM dNTPs, 0.8 μL of each primer (5 μM), 0.4 μL of FastPfu polymerase, and 10 ng of template DNA, and PCR-grade water to adjust the volume. The PCR conditions to amplify the FL prokaryotic 16S rRNA gene consisted of an initial denaturation at 95 ℃ for 2 min; 25 cycles of denaturation at 95 ℃ for 30 s, annealing at 55 ℃ for 30 s, and extension at 72 ℃ for 1 min; and then final extension at 72 ℃ for 5 min.

The PCR products were confirmed with 2% agarose gel electrophoresis, and purified using the AxyPrep DNA Gel Extraction Kit (Axygen Biosciences, USA) according to the manufacturer's instructions. After quantification by QuantiFluor TM-ST (Promega, USA), the amplicon pools were prepared for library construction. SMRTbell libraries were prepared using the Pacific Biosciences SMRTbellTM Template Prep kit 1.0 (PacBio, USA) and sequenced on PacBio RS II (LC-Bio Technology Co., Ltd., Hangzhou, China).

Circular consensus sequence (CCS) reads were generated from raw subreads by SMRT Link (v6.0) with the following parameters: minPasses = 5; minPredictedAccuracy = 0.9. Then lima (v1.7.1) was used to distinguish CCS reads from different samples, and cutadapt (v1.9) was applied to identify primers. The CCS reads between 1200 to 1650 bp remained after the length filtration. After dereplication and filtering chimeric sequences using DADA2, we obtained a feature table and feature sequence. Alpha diversity and beta diversity were calculated by normalizing them to the same sequences randomly. Alpha diversity was applied in analyzing the complexity of species diversity for a sample through five indices, including Chao1, Observed species, Goods coverage, Shannon, Simpson, and all these indices were calculated with QIIME2. Beta diversity was calculated by QIIME2. The ASVs were annotated by aligned feature sequences with the SILVA database (release 138). Other diagrams were implemented using the R packages.

#### Fecal microbiota transplantation (FMT)

In the SPF mice FMT experiment, all mice took pure water as drinking water. Mice were given a four antibiotics cocktail (neomycin sulfate 200 mg/kg, metronidazole 200 mg/kg, ampicillin 200 mg/kg, and vancomycin 100 mg/kg) via oral gavage for 7 consecutive days before FMT to pre-deplete the endogenous gut microbiota. All the antibiotics used here were purchased from Sangon Biotech (Cat. Nos. A610366, A600633, A610028, and A600983; Shanghai, China). FMT was performed once daily for two weeks after a 1-d recovery of antibiotics cocktail. For the FMT experiments, we collected 200–300 mg fresh fecal samples from control mice and mice exposed to CMC between 15:00 and 17:00. Fresh fecal samples were homogenized in PBS, filtered through a 100-μm cell strainer, and centrifuged at 7000 g for 5 min; recipient mice were administered 200 μl of the supernatant via oral gavage. Recipient mice in the FMT-Ctrl/FMT-CMC group received gut microbiota from control mice or mice exposed to CMC for 2 weeks respectively.

#### Germ-free (GF) mice FMT

Germ-free C57BL/6 mice (6–8 weeks) were bred and maintained in special plastic isolators (GemParmatech, Nanjing, China), and experiments were approved by GemParmatech IACUC (GPTAP20221024-4). All mice were housed under a strict 12-h light cycle (lights on at 08:00). Animals were supplied with a 50-kGy irradiated sterile pelleted normal chow diet (Xietong Shengwu, Nanjing, China) and autoclaved tap water ab libitum. Bedding was replaced in all experiments every 7 days. All germ-free mice were routinely screened for bacteria, viral, and fungus contamination.

FMT donor mice were housed in the animal laboratory of Changhai Hospital. The donor mice were either exposed or not exposed to CMC. Donor feces were collected and prepared into fecal microbial suspensions, which were then shipped to the laboratory where germ-free mice were kept. Subsequently, FMT was performed via gavage.

#### 10X Single-cell RNA sequencing: samples and analysis

The whole blood (approximately 0.8 mL) was obtained from each mouse in these two groups ($n = 4$ per group). PBMCs were isolated from whole blood by Ficoll gradient separation [29]. Cell suspensions were then performed for scRNA-seq. The library was established by 10X genomics recommendation for 3′ tag Single Cell Gene Expression (10 × Genomics, Pleasanton, CA). The libraries were sequenced by Illumina HiSeq6000 (Illumina, San Diego, CA). The 10X Single-Cell Software Cell Ranger was used to process raw data, which aligned the sequenced reads under the mm10 mouse reference

genome and quantified single-cell expression level, also removed low-quality reads. A total of 65,960 cells were included in the downstream analysis after quality filtration. Of those cells, 29,951 cells were FMT-Ctrl-derived and 36,009 cells were FMT-CMC-derived.

Downstream analyses were performed by R (4.2.0) and the "Seurat" package (4.1.1) [30]. Cells with < 200 or > 5000 genes or with more than 10% mitochondrial genes were considered low-quality and filtered [31]. Doublets were identified and removed by the package "DoubletFinder" (2.0.1). After quality control, ounts were normalized by "NormalizeData." We used the "Harmony" package (1.0) to minimize batch differences. The top 30 principal components and the top 2000 variable genes were applied. We used the "FindClusters" function of Seurat (resolution = 6) for cell clustering and visualized them by "RunUMAP" function in 2D uniform manifold approximation and projection (UMAP).

Markers of each cell cluster were identified through "FindAllMarker" function. The differentially expressed genes (DEGs) were calculated by "FindMarkers" function. The adjusted $p$ value < 0.01 was used as the cutoff threshold value. The DEGs were then processed by clusterProfiler package (3.18.0) for Gene set enrichment analysis (GSEA) pathways enrichment analysis. Gene set variation analysis (GSVA) was used depending on the C2, C5, KEGG, hallmark, and WP gene set from the molecular signature database, as the instructions of the GSVA package (1.38.0) for each cell with default parameters. The "progeny" package (1.18.0) was applied to analyze several classical pro-inflammatory pathway activities for single cells [32].

To investigate the regulon network, we used pySCENIC, a Python-based algorithm in Jupyter Notebook software (1.0.0), to reconstruct transcription states and regulatory networks from scRNA-SEQ data. We identified differences in area under the curve (AUC) between cells or between modules calculated by SCENIC (1.2.2) of cell clusters. Regulation of $p$ value (adv. P val) > 0.01 was excluded for further study.

In order to explore the transcriptional alternations of FMT-Ctrl and FMT-CMC, we utilized Monocle (2.18.0) for single-cell dramatic pseudotime trajectories [33]. The RNA counts were included in "Monocle2" for analysis. "Differential GeneTest" function was used to build a potential developmental trajectory.

CellphoneDB (based on Python 3.7) [34] and cellchat (1.6.1) [35] were calculation tools for cell–cell communication analysis. The cell clusters were investigated to establish cell interaction networks. The ligand-receptor pairs with a $p$ value < 0.05 were considered to be the significant interaction.

#### Cell culture

The mouse macrophage line RAW264.7 was purchased from Procell Life Science&Technology (Wuhan, China) and cultured with Dulbecco's modified Eagle medium (DMEM) (10,569,044, Gibco, Carlsbad, CA) containing 10% fetal bovine serum (10,099,141, Gibco) and 100 U/mL penicillin and 100 μg/mL streptomycin at 37 °C with 5% $CO_2$.

#### Cell transfection

The RAW264.7 macrophages ($4 \times 10^5$cells/well) were seeded in a 6-well plate. Upon cell confluence reaching 70–80%, cells were grouped and transfected with C/EBPδ overexpression plasmid (oe-C/EBPδ) or plasmids carrying short hairpin RNA targeting C/EBPδ(sh-C/EBPδ). All plasmids and siRNAs (20 uM/uL) were transfected using the Advanced DNA RNA Transfection Reagent™ (ZETA LIFE, USA) according to the manufacturer's protocol. Briefly, plasmid or siRNA was directly mixed with transfection reagent according to 1:1 relationship, then mixed by blowing into a pipette 10–15 times. Following incubation at room temperature for 10–15 min, the complex was added to the cell culture plates, mixed gently, and incubated in the $CO_2$ incubator for 24 h. Sequences and plasmids used were all provided by RiboBio (Shanghai, China).

#### Monocyte C/EBPδ knockdown mice experiment

Cx3cr1-iCre Cas9-KI mice (Strain NO. T006768) were purchased from GemPharmatech (Nanjing, China). Monocyte C/EBPδ knockdown mice were produced by tail vein injection of pAAV-CMV-DIO-EGFP-miR30shRNA(Cebpd)-WPRE into Cx3cr1-iCre Cas9-KI mice. After the injection of AAV, mice were provided with pure water or CMC solution (1%) based on their group assignment for a 28-day intervention period. Following this, acute pancreatitis was induced using caerulein.

#### Quantitative reverse-transcription PCR (qRT-PCR)

The total RNA of tissue and cells was extracted using Trizol reagent (Invitrogen, #15,596,026) according to the manufacturer's instructions. RNA concentration and quality were measured by Nanodrop One Spectrophotometers (Thermo Fisher Scientific). RNA was reverse-transcribed to cDNA using HiScript III RT SuperMix for quantitative RT-PCR (+gDNA wiper) (Vazyme Biotech, R223-01), and qRT-PCR was performed on Lightcycler 480 II system (Roche) using ChamQ Universal SYBR quantitative RT-PCR master mix (Vazyme Biotech, Q711-02). The expression level was normalized to the housekeeping Actb gene, and data were analyzed

using the 2-ΔΔCT method. Primers used in qRT-PCR are shown in Table S2.

#### Quantification of LBP (lipopolysaccharide-binding protein) levels

The serum LBP level was measured with an ELISA kit (Elabscience, E-EL-M3090) according to the manufacturer's instructions.

#### Immunofluorescence assay

Colon sections were deparaffinized, antigen retrieved, blocked, and incubated with antibodies zo-1 (Proteintech, 21,773–1-AP) and claudin-1 (Servicebio, GB112543). After incubation with DAPI, the slides were scanned under a panoramic midi digital slice scanner (3DHISTECN, Budapest, Hungary).

#### Western blot

The total protein of colonic tissue was extracted by RIPA lysis buffer (Beyotime, P0013C) containing proteinase inhibitors cocktail (Epizyme, GRF101). Protein concentrations were determined by the BCA Protein Assay Kit (Beyotime, P0012). Tissue lysates were electrophoresed on SurePAGE 4–12% Bis–Tris gels (GeneScript, M00654), then transferred to Immobilon-P PVDF transfer membrane (Millipore, IPVH00010). Skim milk (BioFroxx, 1172GR500) was used for blocking nonspecific binding sites. The following antibodies were used in western blot: beta actin monoclonal antibody (1:100,000, proteintech, 66,009–1-Ig) as an internal reference, and ZO-1 polyclonal antibody (1 μg/mL, Invitrogen, 61–7300), claudin 1 polyclonal antibody (1:1000, proteintech, 13,050–1-AP) as primary antibodies. The HRP-linked anti-rabbit IgG (1:10,000, WESTANG BIO-TECH, C0151) and HRP-linked anti-mouse IgG (1:10,000, WESTANG BIO-TECH, C0152) were chosen according to the primary antibodies. Signals were visualized using the Immobilon ECL Western Substrate (Millipore, WBKLS0100), and images were acquired using the Amersham Imager 600 system (GE Life Science).

#### Eritoran rescue experiment

Mice were divided into four groups: Ctrl, Ctrl + Eritoran, CMC, and CMC + Eritoran. In Ctrl and Ctrl + Eritoran groups, mice took pure water for 28 days, and on day 28, the Ctrl group received an intraperitoneal injection of NS (100 μl), while the Ctrl + Eritoran group received an intraperitoneal injection of Eritoran (2.33 mg/ml, 100 μl) (MCE, 185,955–34-4). In CMC and CMC + Eritoran groups, mice took CMC solution (1%) for 28 days. On day 28, the CMC group received an intraperitoneal injection of NS (100 μl), while the CMC + Eritoran group received an intraperitoneal injection of Eritoran (2.33 mg/ml, 100 μl) (MCE, 185,955–34-4). One hour after the injection of NS or Eritoran, AP was induced in all four groups using caerulein.

#### Flow cytometry and antibodies

PBMCs were isolated from whole blood by Ficoll gradient separation. Cell viability and cell surface marker staining were performed at 4 °C in the dark at first. When cell staining was completed, cells were acquired and detected with the CytoFLEX Flow Cytometer (Beckman Coulter). FlowJo v.10 (TreeStar) was used for data analysis. The antibodies used in the flow cytometry analysis were all sourced from Invitrogen: anti-CD45 (BioLegend, 103,107); anti-CD11b (BioLegend, 101,212); anti-Ly-6C (BioLegend, 128,007); and anti-Ly-6G (BioLegend, 127,628).

#### Short-chain fatty acid (SCFA) quantification analysis

Feces (20 mg per mouse) (excluding intestinal tissue) were homogenated for 1 min with 500 μL of water and 100 mg of glass beads and then centrifuged at 4 ℃ for 10 min at 12,000 rpm. Two hundred microliter supernatant was extracted with 100 μL of 15% phosphoric acid and 20 μL of 375 μg/mL 4-methylvaleric acid solution as IS and 280 μL ether. Subsequently, the samples were centrifuged at 4 ℃ for 10 min at 12,000 rpm after vortexing for 1 min and the supernatant was transferred into the vial prior to GC–MS analysis. The extracted samples were detected using trace 1310 gas chromatograph (Thermo Fisher Scientific, USA) and ISQ 7000 (Thermo Fisher Scientific, USA). SCFA standards were mixtures of acetate, propionate, butyrate, isobutyrate, valerate, isovalerate, and hexanoate. All the standards were purchased from Sigma (Darmstadt, Germany).

#### Butyrate rescue experiment

In the Ctrl group, mice were provided with pure water for a duration of 28 days, whereas mice in the CMC/CMC + Butyrate group were administered a 1% CMC solution over the same period. From day 14 to day 28, mice in the CMC + Butyrate group underwent daily gavage with butyrate (200 mg/kg/d, Sigma-Aldrich, 303,410), while mice in the Ctrl/CMC group received daily gavage with pure water. AP was induced on day 28.

#### Akkermansia muciniphila administration and quantification

*Akkermansia muciniphila* was purchased from ATCC (ATCC Number: BAA-835) and cultured in 0.5% (wt/vol) mucin-supplemented brain heart infusion (BHI) (Difco, MI, USA) medium anaerobically at 37 °C. After 48 h of incubation, the cultures were centrifuged at 7000 g for 15 min, washed twice in sterile saline, and resuspended at a

bacterial concentration of $1.5\times10^{10}$ CFU/mL by measuring absorbance at 630 nm for further intragastric administration. Mice in the CMC + AKK group were orally gavaged with $3\times10^{9}$ CFU *Akkermansia muciniphila* suspended in 0.2 mL of PBS per day, while mice in the Ctrl and CMC groups were treated with an equivalent dose of PBS. The treatments were administered for 14 days.

*Akkermansia muciniphila* quantification was detected by qRT-PCR, and the relative abundance of *Akkermansia muciniphila* was calculated using the previously published method [36]. The primers used in quantification: Total Bacteria (Bacteria Universal) F-ACTCCTACGGGAGGCAGCAG, R-ATTACCGCGGCTGCTGG; *Akkermansia muciniphila* F-CAGCACGTGAAGGTGGGGAC, R-CCTTGCGGTTGGCTTCAGAT.

### Patient and public involvement statement

Patients were included from July 15, 2023, to August 15, 2023. A total of 54 newly diagnosed AP patients, including 23 mild AP (MAP), 12 moderate severe AP, and 19 severe AP, were enrolled for full-length 16s rRNA sequencing. Severity was defined as MAP (mild), MSAP (moderate severe), or SAP (severe) according to the revised Atlanta criteria. Information regarding age and sex is recorded in Table S3 for each individual patient. The exclusion criteria of this study were as follows: antibiotic/probiotics usage within 3 months and chronic gastrointestinal diseases. All patients provided written informed consent. The study was approved by the Shanghai Changhai Hospital Ethics Committee (CHEC2023-159).

### Statistical analysis

Numeric data were expressed as mean ± S.E.M, data with normal distribution were compared by Student's *t*-test, while data with abnormal distribution were compared by Wilcoxon rank-sum test. $p<0.05$ was considered statistically significant. All statistical analyses were performed on GraphPad Prism v9.3.1 and R v4.0.2 software.

#### Abbreviations

| | |
|---|---|
| AP | Acute pancreatitis |
| BISAP | Bedside index for severity in acute pancreatitis |
| C/EBPδ | CCAAT/enhancer-binding protein delta |
| CAE | Caerulein |
| CMC | Carboxymethylcellulose |
| ELISA | Enzyme-linked immunosorbent assay |
| FMT | Fecal microbiota transplantation |
| GF | Germ free |
| GSEA | Gene set enrichment analysis |
| GSVA | Gene set variation analysis |
| LPS | Lipopolysaccharide |
| MAP | Mild acute pancreatitis |
| MSAP | Moderate severe acute pancreatitis |
| NS | Normal saline |
| PBMCs | Peripheral blood mononuclear cells |
| PCoA | Principal coordinates analysis |
| qRT-PCR | Quantitative reverse-transcription PCR |
| SAP | Severe acute pancreatitis |
| SCFAs | Short chain fatty acids |
| scRNA-seq | Single-cell RNA sequencing |
| siRNA | Small interfering RNA |
| SPF | Specific pathogen free |
| UPFs | Ultra processed foods |
| ZO-1 | Zonula occludens-1 |

## Supplementary Information

The online version contains supplementary material available at https://doi.org/10.1186/s40168-025-02074-1.

Additional file 1: Supplementary figure.

Additional file 2: Supplementary tables.

#### Acknowledgements

We thank Shanghai Zhi Bei Biotechnology Co., Ltd. and Shanghai Biotree Biotech Co., Ltd. for bioinformatics analysis and data processing.

#### Authors' contributions

YF: study design, performing experiments, data analysis, and manuscript writing. WC: performing experiments, and data analysis. JC: performing experiments, and data analysis. FS: performing experiments, and data analysis. FK: performing experiments, and data analysis. LL: performing experiments, and data analysis. YZ: performing experiments. SW: data analysis. ZL: study design, data interpretation, manuscript writing, and overall supervision. YD: study design, data interpretation, manuscript writing, and overall supervision. XK: study design, data interpretation, manuscript writing, and overall supervision.

#### Funding

Supported in part by grants 82072760 and 81772640 (X.K.), 82170659 (Y.D.), 82372923 (F.K.), 81872043 and 82172572 (L.L.) from the National Natural Science Foundation of China; National Key R&D Program of China No. 2019YFC1315900 and SQ2024YFC3600112.

#### Data availability

The raw sequence data reported in this paper have been deposited in the Genome Sequence Archive (Genomics, Proteomics & Bioinformatics 2021) in National Genomics Data Center (Nucleic Acids Res 2022), China National Center for Bioinformation / Beijing Institute of Genomics, Chinese Academy of Sciences (BioProject: PRJCA022643) that are publicly accessible at https://ngdc.cncb.ac.cn/gsa.

## Declarations

#### Ethics approval and consent to participate

The study was approved by the Shanghai Changhai Hospital Ethics Committee (CHEC2023-159). All patients provided written informed consent.

#### Consent for publication

Not applicable.

#### Competing interests

The authors declare no competing interests.

#### Author details

[1]National Key Laboratory of Immunity and Inflammation, Naval Medical University, Shanghai 200433, China. [2]Shanghai Institute of Pancreatic Diseases, Shanghai 200433, China. [3]Department of Urology, Xinhua Hospital, Shanghai Jiaotong University, School of Medicine, Shanghai 200092, China. [4]Changhai Clinical Research Unit, Naval Medical University, Shanghai 200433, People's Republic of China. [5]Digestive Endoscopy Center, Shanghai Tenth People'S Hospital, Tongji University School of Medicine, Shanghai 200433, China. [6]Shanghai Zhenwei Biotechnology Co., Ltd, Shanghai 200245, China.

Received: 7 March 2024 Accepted: 27 February 2025
Published online: 24 March 2025

**References**

1. Srour B, Kordahi MC, Bonazzi E, Deschasaux-Tanguy M, Touvier M, Chassaing B. Ultra-processed foods and human health: from epidemiological evidence to mechanistic insights. Lancet Gastroenterol Hepatol. 2022;7:1128–40.
2. Sellem L, Srour B, Javaux G, Chazelas E, Chassaing B, Viennois E, et al. Food additive emulsifiers and risk of cardiovascular disease in the NutriNet-Santé cohort: prospective cohort study. BMJ. 2023;382:e076058.
3. Fiolet T, Srour B, Sellem L, Kesse-Guyot E, Allès B, Méjean C, et al. Consumption of ultra-processed foods and cancer risk: results from NutriNet-Santé prospective cohort. BMJ. 2018;360: k322.
4. Chassaing B, Compher C, Bonhomme B, Liu Q, Tian Y, Walters W, et al. Randomized controlled-feeding study of dietary emulsifier carboxymethylcellulose reveals detrimental impacts on the gut microbiota and metabolome. Gastroenterology. 2022;162:743–56.
5. Chassaing B, Koren O, Goodrich JK, Poole AC, Srinivasan S, Ley RE, et al. Dietary emulsifiers impact the mouse gut microbiota promoting colitis and metabolic syndrome. Nature. 2015;519:92–6.
6. Chassaing B, Van de Wiele T, De Bodt J, Marzorati M, Gewirtz AT. Dietary emulsifiers directly alter human microbiota composition and gene expression ex vivo potentiating intestinal inflammation. Gut. 2017;66:1414–27.
7. Naimi S, Viennois E, Gewirtz AT, Chassaing B. Direct impact of commonly used dietary emulsifiers on human gut microbiota. Microbiome. 2021;9:66.
8. Mederos MA, Reber HA, Girgis MD. Acute pancreatitis: a review. JAMA. 2021;325:382–90.
9. Daniel N, Gewirtz AT, Chassaing B. Akkermansia muciniphila counteracts the deleterious effects of dietary emulsifiers on microbiota and host metabolism. Gut. 2023;72:906–17.
10. van den Berg FF, van Dalen D, Hyoju SK, van Santvoort HC, Besselink MG, Wiersinga WJ, et al. Western-type diet influences mortality from necrotising pancreatitis and demonstrates a central role for butyrate. Gut. 2021;70:915–27.
11. Lei Y, Tang L, Liu S, Hu S, Wu L, Liu Y, et al. Parabacteroides produces acetate to alleviate heparanase-exacerbated acute pancreatitis through reducing neutrophil infiltration. Microbiome. 2021;9:115.
12. Zhu Q, Yuan C, Dong X, Wang Y, Li B, Tu B, et al. Bile acid metabolomics identifies chenodeoxycholic acid as a therapeutic agent for pancreatic necrosis. Cell Rep Med. 2023;4(12):101304.
13. Lu Y, Yuan X, Wang M, He Z, Li H, Wang J, et al. Gut microbiota influence immunotherapy responses: mechanisms and therapeutic strategies. J Hematol Oncol. 2022;15:47.
14. Wastyk HC, Fragiadakis GK, Perelman D, Dahan D, Merrill BD, Yu FB, et al. Gut-microbiota-targeted diets modulate human immune status. Cell. 2021;184:4137-4153.e14.
15. Manohar M, Jones EK, Rubin SJS, Subrahmanyam PB, Swaminathan G, Mikhail D, et al. Novel circulating and tissue monocytes as well as macrophages in pancreatitis and recovery. Gastroenterology. 2021;161:2014-2029.e14.
16. Liu Y-W, Chen C-C, Wang J-M, Chang W-C, Huang Y-C, Chung S-Y, et al. Role of transcriptional factors Sp1, c-Rel, and c-Jun in LPS-induced C/EBPdelta gene expression of mouse macrophages. Cell Mol Life Sci. 2007;64:3282–94.
17. Canfora EE, Jocken JW, Blaak EE. Short-chain fatty acids in control of body weight and insulin sensitivity. Nat Rev Endocrinol. 2015;11:577–91.
18. Depommier C, Everard A, Druart C, Plovier H, Van Hul M, Vieira-Silva S, et al. Supplementation with Akkermansia muciniphila in overweight and obese human volunteers: a proof-of-concept exploratory study. Nat Med. 2019;25:1096–103.
19. Zhang XM, Zhang ZY, Zhang CH, Wu J, Wang YX, Zhang GX. Intestinal microbial community differs between acute pancreatitis patients and healthy volunteers. Biomed Environ Sci. 2018;31:81–6.
20. Tan C, Ling Z, Huang Y, Cao Y, Liu Q, Cai T, et al. Dysbiosis of intestinal microbiota associated with inflammation involved in the progression of acute pancreatitis. Pancreas. 2015;44:868–75.
21. Zhu Y, He C, Li X, Cai Y, Hu J, Liao Y, et al. Gut microbiota dysbiosis worsens the severity of acute pancreatitis in patients and mice. J Gastroenterol. 2019;54:347–58.
22. Narasimhan PB, Marcovecchio P, Hamers AAJ, Hedrick CC. Nonclassical monocytes in health and disease. Annu Rev Immunol. 2019;37:439–56.
23. Li Y, Huang X, Huang S, He H, Lei T, Saaoud F, et al. Central role of myeloid MCPIP1 in protecting against LPS-induced inflammation and lung injury. Signal Transduct Target Ther. 2017;2:17066.
24. Younan P, Ramanathan P, Graber J, Gusovsky F, Bukreyev A. The toll-like receptor 4 antagonist eritoran protects mice from lethal filovirus challenge. mBio. 2017;8:e00226–17.
25. van Minnen LP, Timmerman HM, Lutgendorff F, Verheem A, Harmsen W, Konstantinov SR, et al. Modification of intestinal flora with multispecies probiotics reduces bacterial translocation and improves clinical course in a rat model of acute pancreatitis. Surgery. 2007;141:470–80.
26. Gou S, Yang Z, Liu T, Wu H, Wang C. Use of probiotics in the treatment of severe acute pancreatitis: a systematic review and meta-analysis of randomized controlled trials. Crit Care. 2014;18:R57.
27. Besselink MG, van Santvoort HC, Buskens E, Boermeester MA, van Goor H, Timmerman HM, et al. Probiotic prophylaxis in predicted severe acute pancreatitis: a randomised, double-blind, placebo-controlled trial. Lancet. 2008;371:651–9.
28. Zhu Y, Mei Q, Fu Y, Zeng Y. Alteration of gut microbiota in acute pancreatitis and associated therapeutic strategies. Biomed Pharmacother. 2021;141: 111850.
29. Asarat M, Apostolopoulos V, Vasiljevic T, Donkor O. Short-chain fatty acids produced by synbiotic mixtures in skim milk differentially regulate proliferation and cytokine production in peripheral blood mononuclear cells. Int J Food Sci Nutr. 2015;66:755–65.
30. Butler A, Hoffman P, Smibert P, Papalexi E, Satija R. Integrating single-cell transcriptomic data across different conditions, technologies, and species. Nat Biotechnol. 2018;36:411–20.
31. Chen W, Dong K, Pan X, Gan S, Xu D, Chen J, et al. Single-cell RNA-seq integrated with multi-omics reveals SERPINE2 as a target for metastasis in advanced renal cell carcinoma. Cell Death Dis. 2023;14:30.
32. Schubert M, Klinger B, Klünemann M, Sieber A, Uhlitz F, Sauer S, et al. Perturbation-response genes reveal signaling footprints in cancer gene expression. Nat Commun. 2018;9:20.
33. Qiu X, Hill A, Packer J, Lin D, Ma Y-A, Trapnell C. Single-cell mRNA quantification and differential analysis with Census. Nat Methods. 2017;14:309–15.
34. Efremova M, Vento-Tormo M, Teichmann SA, Vento-Tormo R. Cell PhoneDB: inferring cell–cell communication from combined expression of multi-subunit ligand–receptor complexes. Nat Protoc. 2020;15:1484–506.
35. Jin S, Guerrero-Juarez CF, Zhang L, Chang I, Ramos R, Kuan C-H, et al. Inference and analysis of cell-cell communication using Cell Chat. Nat Commun. 2021;12:1088.
36. Bacchetti De Gregoris T, Aldred N, Clare AS, Burgess JG. Improvement of phylum- and class-specific primers for real-time PCR quantification of bacterial taxa. J Microbiol Methods. 2011;86:351–6.

## Publisher's Note